JOURNAL OF SPACECRAFT AND ROCKETS
Vol. 46, No. 3, May–June 2009

Investigation of Missile-Shaped Body with Forward-Facing Cavity at Mach 8

S. Saravanan,* G. Jagadeesh,† and K. P. J. Reddy‡
Indian Institute of Science, Bangalore 560 012, India

DOI: 10.2514/1.38914

A blunt-nosed hypersonic missile mounted with a forward-facing cavity is a good alternative to reduce the stagnation heating rates. The effects of a forward-facing cavity on heat transfer and aerodynamic coefficients are addressed in this paper. Tests were carried out in hypersonic shock tunnel HST2, at a hypersonic Mach number of 8 using a 41 deg apex-angle blunt cone. The aerodynamic forces on the test model with and without a forward-facing cavity at various angles of attack are measured by using an internally mountable accelerometer force balance system. Heat flux measurements have been carried out on the test model with and without a forward-facing cavity of the entire surface at zero degree angle of attack with platinum sensors. A numerical simulation was also carried out using the computational fluid dynamics code (CFX-Ansys 5.7). An important result of this study is that the smaller cavity diameter has the highest lift-to-drag ratio, whereas the medium cavity has the highest heat flux reduction. The shock structure around the test model has also been visualized using the Schlieren flow visualization technique. The visualized shock structure and the measured aerodynamic forces on the missile-shaped body with cavity configurations agree well with the axisymmetric numerical simulations.

Nomenclature

a, b	=	locations of the accelerometers from the center of gravity of the model
C_d	=	drag force coefficient
C_l	=	lift force coefficient
C_m	=	pitching moment coefficient
$C(t)$	=	axial force
D	=	cavity diameter
D_B	=	model base diameter
g	=	acceleration due to gravity, 9.81 m/s^2
H_0	=	stagnation enthalpy
L	=	cavity length
m	=	mass of the model
M_∞	=	freestream Mach number
M_s	=	shock Mach number
$N(t)$	=	normal force
P_0	=	stagnation pressure
P_∞	=	freestream static pressure
q_∞	=	freestream dynamic pressure
$q(t)$	=	heat flux at time t
$R_{e\infty}$	=	freestream unit Reynolds number
R_n	=	model nose radius
St	=	Stanton number
t	=	time
T_0	=	stagnation temperature
T_∞	=	freestream static temperature
V_∞	=	freestream velocity
α	=	angle of attack
ξ_1, ξ_2, ξ_3	=	measured accelerations
ρ_∞	=	freestream static density

Received 3 June 2008; revision received 12 January 2009; accepted for publication 3 February 2009.

*Senior Scientific Officer, Department of Aerospace Engineering (Corresponding Author).
†Associate Professor, Department of Aerospace Engineering. Member AIAA.
‡Professor, Department of Aerospace Engineering.

I. Introduction

FOR any vehicle flying in the Earth's atmosphere, the design objectives must be tailored to the required mission and flight conditions. A commercial aircraft, for example, is designed for a cost-effective flight. In contrast, economical flight requirements are irrelevant for an armed missile, which should be capable of achieving its mission. New concepts on supersonic and hypersonic missiles are in progress worldwide for both short-range air defense guided missiles as well as long-range interceptor missiles, including reentry vehicles and hypersonic aircraft. The overall drag force experienced by aerospace vehicles at hypersonic flight speeds is predominately due to the formation of strong shock waves in the flow. In addition, aerodynamic drag and high heating associated with shocks at leading edges are significant issues. For example, beyond Mach 3 missile leading edges are exposed to high heating rates causing high temperatures on the structure. In addition to surface melting and ablation, the flight aerodynamics can be perturbed, leading to unacceptable flight trajectory deviations. Another problem is signal refraction passing through the shocked hot gas layer in front of the missile's seeker head. The preferred shape for these purposes is a hemispherical nose, which becomes critically loaded by thermal stresses at the nose tip. Therefore, it is of utmost importance to find techniques to reduce the heat at the nose tip of a high-speed missile. Most of the high-speed vehicles have therefore traditionally tended to recommend a hemispherical nose, which becomes critically loaded by thermal stresses at the nose tip. To weaken the shock system and specifically reduce resultant pressurization on upstream-facing vehicle surfaces, various techniques, such as retractable aerospikes ahead of the blunt body [1], concentrated energy deposition along the stagnation streamline [2], and forward-facing jets in the stagnation zone of a blunt body [3] are being investigated by many researchers around the globe for keeping the heat load and drag of the missile body to acceptable levels. However, disadvantages of the preceding techniques are structural problems and flow disturbance.

Among all these techniques, use of a forward-facing cavity appears to be the simplest to reduce the heat, and, at the same time, it can be used to increase the lift-to-drag ratio. Hence, in the present investigation, we have focused on the forward-facing cavity to reduce heat loads as well as for the possibility of drag forces for stability and control purposes.

Recently, several papers [4–6] have appeared involving the use of a forward-facing cavity in the nose tip of a projectile to reduce stagnation-point heating. Since the late fifties, cavity flows have been the subject of many investigations, and reviews of some of the

important studies are listed here. One technique, introduced by Hartmann and Troll [7] in 1922 for producing sound of high intensity and discrete frequency, is known as the "Hartmann whistle." This concept involves the flow of a supersonic jet over a body containing a forward-facing cavity. Research efforts related to these ideas have been reviewed by a number of researchers, and in 1959 Burbank and Stallings [8] reported that the stagnation-point heat transfer rate for a concave axisymmetric nose cone at supersonic Mach numbers is considerably lower than that of a convex nose cone. Johnson [9] investigated the flowfield associated with hypersonic helium flow over blunt bodies with surface cavities and found a very violent instability to be connected with these cavities. Baysal and Stallings [10] carried out a 2-D Navier–Stokes analysis using an upwind relaxation scheme to compute the flow at the half-width symmetry plane of the cavity. Marquart and Grubb [11] performed a hypersonic wind tunnel test at Arnold Engineering Development Centre to investigate the dynamics of a detached bow shock, acoustic resonance in the forward-facing nose cavity of a blunt-faced model, and oscillations of the bow shock in front of the cavity (i.e., by using a laser interferometer). Huebner and Utreja [12] reported on heat fluxes for a nose-cavity arrangement, which were found to be less significant at the base of a cavity than at the outer edge. Later, they investigated [4] that the bow-shock oscillation frequency and amplitude were directly related to the cavity depth.

Experiments at Mach 5 [13] using an infrared camera indicated that larger-diameter shallow cavities created a stable "cool ring" in the vicinity of the cavity lip, with temperatures locally lower than those of a simple spherical nose. Fluctuating pressure measurements made at the center of the cavity base showed that oscillations inside the cavity had dominant frequencies that were close to classic organ pipe values. Morgenstern and Chokani [14,15] investigated the hypersonic flow over a cavity. The objective of the study is to investigate the effects of Reynolds number and cavity dimension. Silton and Goldstein [16,17] used an axial cavity at the nose tip of a hypersonic vehicle to reduce the severe heating and delay the ablation onset. In addition, they investigated the impact of the cavity on aerodynamic drag. The effects of nose-tip heat reduction by a forward-facing cavity at the nose of a supersonically flying vehicle, has been published by Engblom et al [18–21]. Engblom and Goldstein [22] published an interesting result on the cooling benefit reached through geometry optimization, finding that "rounding the cavity lip is necessary to reduce local surface heating since the airflow into the cavity directly impinges on the cavity lip."

Based on this knowledge, a study was initiated in IISc (Indian Institute of Science) to determine heating rates near the stagnation region in the presence of a cavity for a missile geometry, which is today strongly relevant for supersonic and hypersonic seeker head configurations. The main goal of the present investigation is to determine the heat fluxes as they exist in real conditions. For these studies, three missile head mock-ups, as shown in Fig. 1, were chosen, designed, and manufactured. Figure 1a duplicates classically designed blunt head geometry without a cavity, and the other two are generic cavity-nosed missile configurations. Figure 1b represents a cavity with medium diameter, whereas Fig. 1c shows a head design with a significantly bigger diameter. For the test-dome in Fig. 1b the cavity diameter is 6 mm and for Fig. 1c it is 12 mm.

The main objectives of the present study are 1) design and fabrication of an internally mountable three-component accelerometer balance system for measuring the fundamental aerodynamic force coefficients for forward-facing cavities, 2) visualization of the shock structure around missile-shaped body with and without a cavity using the schlieren technique, 3) evaluation of cavity dimension as a possible heat reduction device and the effect of a cavity on aerodynamic drag force for a missile body, 4) measurement of convective heat transfer rates to the missile shaped body (i.e., with and without cavity) by using vacuum sputtered platinum thin-film sensors, and 5) to perform illustrative numerical simulations using commercial computational fluid dynamics (CFD) code to complement the experimental results. The details of this study are discussed in the subsequent sections.

II. Model Configuration

A hemispherically blunted nose cone with a cylinder, frustum, and fins and an axial cavity of length L and diameter D is shown in Fig. 2. Length of the cavity was defined as the length from the nose lip to the cavity base. This configuration has been used for the reduction of heat transfer and drag reduction studies for the present investigation. The basic model is typically a blunted cone–cylinder–frustum with fins configuration and a 20.5 deg cone half-angle and radius of 15 mm, which is nothing but a typical nose tip of the hypersonic missile. The outer cavity edge is rounded, as proposed in [16,22], in order to reduce the local heating. Numerical investigation [16] has been carried out on several geometries, and each cavity geometry used a five zone multiblock flowfield grid. We have not optimized the cavity diameter to the nose diameter for the present investigation; however, parametric study has been made to determine the cavity geometry that could result in a drop in the heat transfer rate (surface heating) without increasing the drag. The cavity has a length of 24 mm. Their length/diameter ratios (L/D) are two and four. A circle of radius of 15 mm is used to fabricate the lip radius (r) for both the cavities. The cavities are made up of aluminum alloy. The nose cone (cavity) has the provisions to accommodate a drag accelerometer and thick Macor inserts. The circular cavity shown in Fig. 2 is attached to the cylinder–frustum portion of the model with triangular fins by means of threads, and Fig. 3 shows the photographic view of the missile-shaped body mounted with a forward-facing cavity. An array of platinum thin-film gauges (Fig. 3a) deposited on thermally insulating backing material flush mounted on the model surface is used for convective surface heat transfer measurements, and an internally mountable accelerometer-based balance system (Fig. 3b) is used for measuring the aerodynamic forces in the investigation.

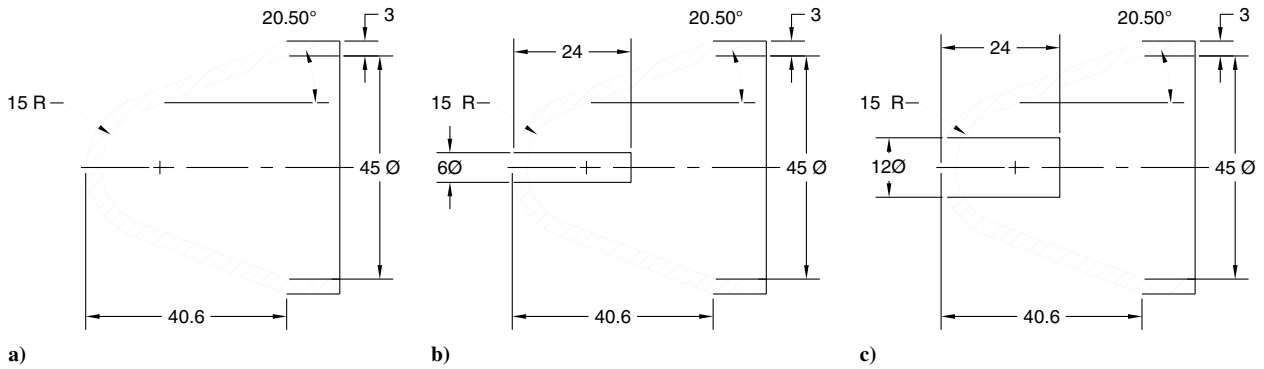

Fig. 1 Design of test dome.

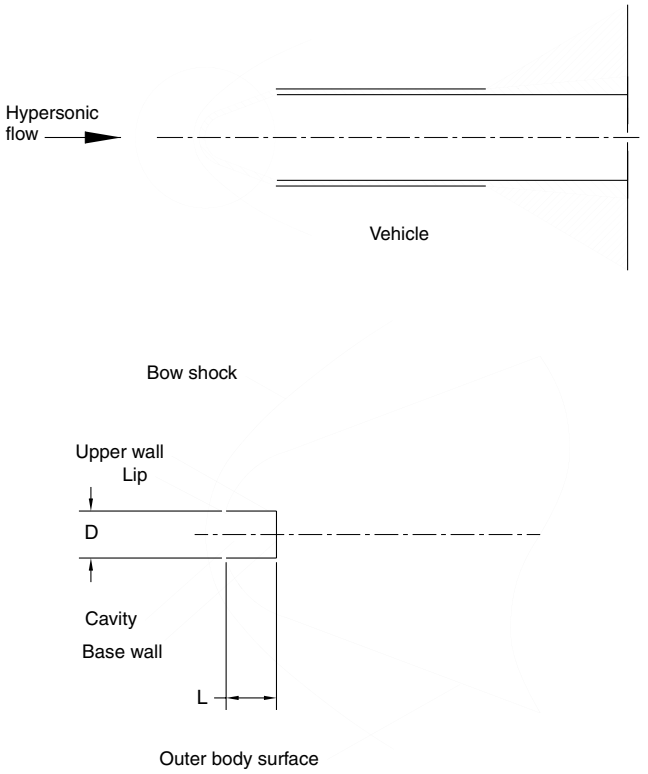

Fig. 2 Schematic of axial cavity in the nose region of a hypersonic vehicle.

III. Experiments

A brief description of the major components of the test facility are given. In addition, experiments on flow visualization, heat transfer, and aerodynamic forces are discussed in detail.

A. Facility Description and Instrumentation

The experimental test facility (HST2) has the capability to supply shock heated air at a maximum stagnation pressure of 40 bar and stagnation temperature of approximately 4000 K. In the present investigation, it is operated in the reflected mode with a convergent–divergent conical nozzle. A principle sketch of HST2 is shown in Fig. 4 with the arrangement of the shock tube, nozzle, test section, and dump tank. The shock tube (Fig. 4) has an internal diameter of 0.051 m, a length of 7.12 m, and is divided into driver (usually filled with highly pressurized helium gas) and driven sections (low-pressure test gas) by an aluminum diaphragm. A Mylar diaphragm divides the driven section from the wind tunnel, which is at an even lower pressure (10^{-5} mbar). Shock velocity in the driven section of the shock tube is measured by using two pressure transducers of 1000 psi range (Model 113A24, PCB-Piezotronics, Ltd.) mounted 0.525 m apart at the end of the driven section. The pressure behind the primary and the reflected shock waves is measured using a pressure transducer (Model 113A22, PCB-Piezotronics, Ltd.) located at end of the driven section. The wind-tunnel portion of the HST2 shock tunnel consists of a truncated conical nozzle terminating into a 30×30 cm size test section, which is attached to a dump tank of about 1 m^3 volume. A nozzle of 10 deg cone angle (706-mm long) with an entrance diameter of 50.8 mm and an exit diameter of 300 mm yields a flow Mach number of 5.75. This is verified by means of a pitot survey across the flow cross section at the nozzle exit. The freestream Mach number can be varied in the reflected mode by adding a convergent–divergent portion with different throat inserts, which produces a range of Mach numbers from 8 to 13 and only a Mach 8 nozzle is used in the present test. The wind tunnel section is usually evacuated before every run using a rotary-roots pump combination. The tunnel is capable of producing a reservoir enthalpy of approximately 4 MJ/kg with an effective test time of approximately 1 ms. Figure 5 shows a pressure history indicating the steady-state test time in the tunnel test section, along with a stagnation pressure measured at end of the shock tube. The typical test condition of the experiment is given in Table 1.

All the data are sampled digitally, using a 12-bit multichannel system (NI PXI-6115 DAS, NI Systems Private Limited), and data are recorded at 1 MHz/channel. Each channel has an amplifier, analog-to-digital converter, 32 K memory, and control circuitry for trigger and timing along with necessary software. All the data during the shock tunnel testing are sampled at a frequency of 1 MHz. The control software is provided with a graphical interface screen.

Introducing a forward-facing cavity ahead of the missile-shaped body flying at a hypersonic Mach number will induce pronounced unsteady shock oscillations in the flowfield. Therefore, before we look for quantitative measurements on cavity models, it is very essential to know about the shock structure of the missile model with the cavity. Hence, in the present study, the shock structure around the cavity model is visualized before the convective heat transfer and force measurements.

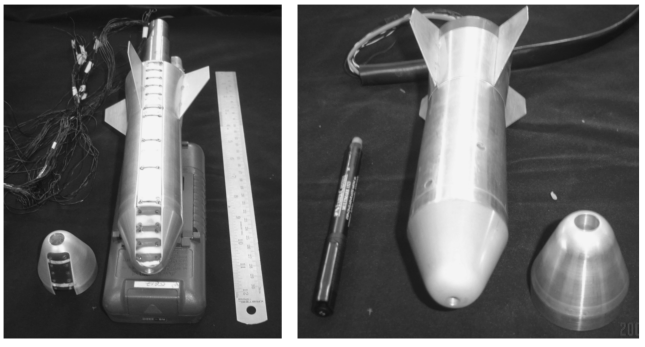

a) b)

Fig. 3 A missile-shaped model with forward-facing cavity fitted with a) platinum thin-film gauges for heat transfer measurements and b) three-component accelerometer balance system for the measurement of aerodynamic coefficients.

B. Flow Visualization Experiments

The test model with and without a cavity used in this experiment is fabricated using duralumin. The hypersonic flow in the test section is captured through the optical quality windows using a high-speed camera. Flow visualizations with schlieren as described in [23] have been used for the present investigation. The schlieren system used for the present visualization has a light source emitting the light and then collimated by using a combination of plane and first collimating mirrors so that parallel rays pass through the optical quartz window of the test section. A second collimating mirror located at other side of the optical window station collects the light passing through the test section then reflected from the plane mirror and produces an image of the light source at a knife edge mounted on an X-Y positioner. Finally, the image of the test section (i.e., model) is captured in the high-speed digital camera (phantom 7.1, M/s Vision Research), and for the present investigation they have been recorded at a speed of 12,048 frames per second at a resolution of 400×400 pixel using a SR-CMOS imaging array. The knife edge is oriented parallel to the freestream flow. The knife edge is moved into or out of the beam. The density gradients around the model will cause refraction of the light rays when a model is present in the test section.

The flow visualization study is carried out for different model configurations (i.e., nose cone without cavity, cavity with 6 and 12 mm). In general, the flow over a test model without cavity configuration is a steady-state flow. However, in the presence of a cavity, the flow is oscillating about the resonant frequency. These frequencies are calculated from a classical organ pipe theory (5662 Hz for 6 mm cavity and 5619 Hz for 12 mm cavity). As a result, both the cavities have shown an oscillatory motion (6 mm cavity results are not shown here). Figure 6 shows the visualized flowfield around the test model (i.e., nose cone) with a 12 mm forward-facing

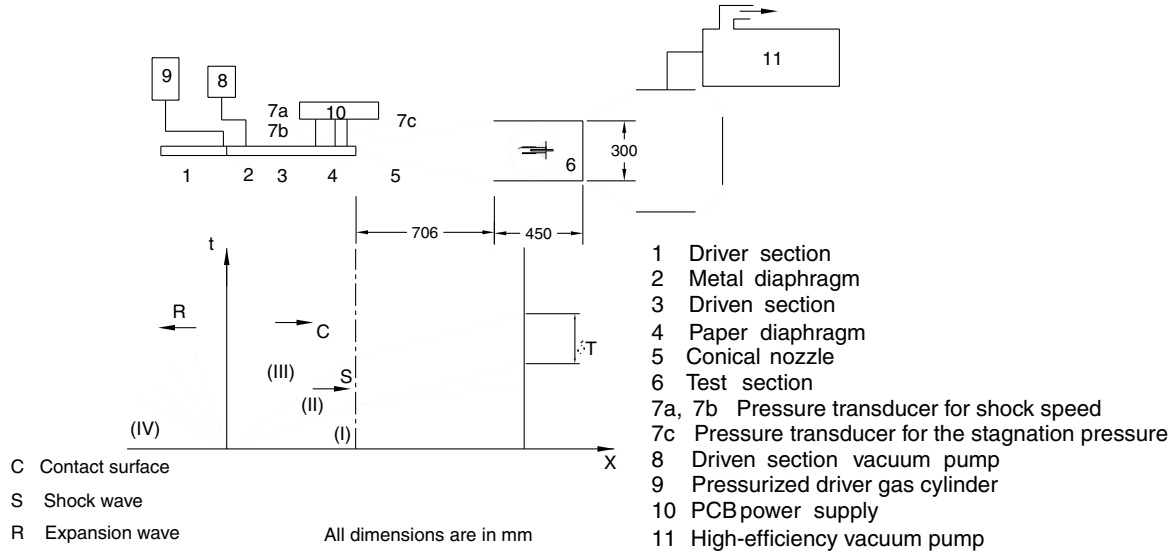

Fig. 4 Schematic diagram of the IISc hypersonic shock tunnel HST2.

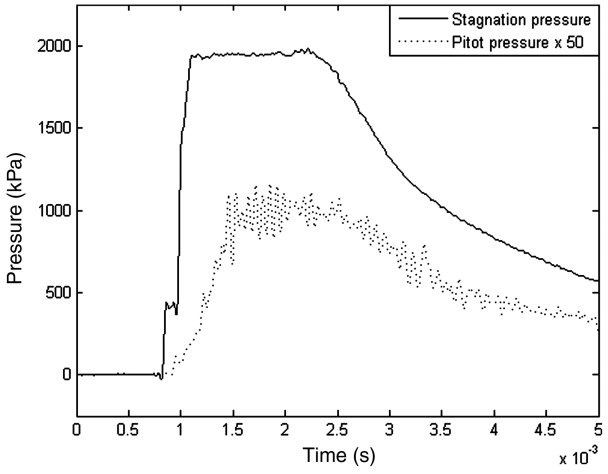

Fig. 5 The typical variation of pitot pressure recorded during the experiment along with the corresponding stagnation pressure variation.

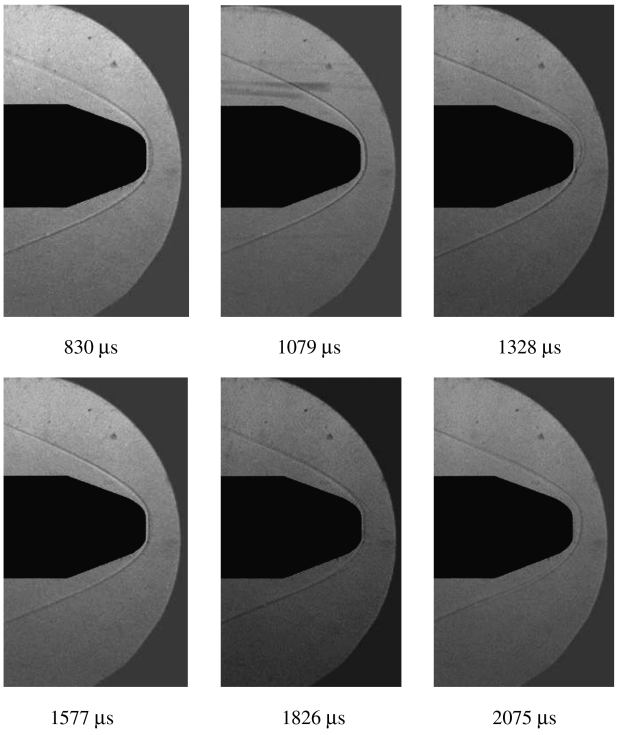

Fig. 6 Schlieren picture of the flowfields for a missile model with a 12 mm cavity flying at Mach 8.

cavity. In the 12 mm cavity configuration, stronger flow gradients develop in front of the cavity. On some of the photographs, we see that the shock waves are able to penetrate into the cavity and few images illustrate nearly steady-state conditions. A similar flow formation has been noticed for the 6 mm cavity case (not shown here), however, a shock wave is moving back and forth in accordance with the cavity pressure. It shows the formation of stationary bow shock in front of the cavity-equipped test model with a flow duration of about 2.5 ms. The shock wave pattern around the test model (without cavity) consists of a stationary, stronger bow shock, and the shock wave is spherical in shape and symmetrical over the forebody of the cone. It shows a series of flow pictures, where light intensity variations represent density variations.

Experimental results of cavity configuration give a hint that the periodic oscillation of bow-shock behavior of a 12 mm cavity is much faster than a 6 mm cavity. The shock is steady for a model without a cavity and oscillation strength increases with a cavity L/D. Also, the position of the bow shock wave is not stationary for both the cavities. The oscillations are dominated by a quarter-wave frequency of the cavity [19], and oscillation strength increases with cavity depth. The interaction of pressure behind the normal shock with the cavity pressure generates a growing pocket of turbulent high-pressure fluid in the region behind the normal shock, which pushes this main bow shock slowly upstream.

Table 1 Test conditions achieved in a HST2 hypersonic shock tunnel

Driver gas	Helium
Primary diaphragm thickness, mm	1.5
Shock Mach number, M_S	3.6
Stagnation pressure P_0, kPa	1940
Stagnation enthalpy H_0, MJ/kg	1.965
Freestream Mach number M_∞	7.96
Freestream static pressure P_∞, Pa	205.2
Freestream static temperature T_∞, K	143
Freestream static density ρ_∞, kg/m^3	0.0049
Freestream velocity V_∞, m/s	1908
Freestream unit Reynolds number Re_∞, m^{-1}	0.98×10^6

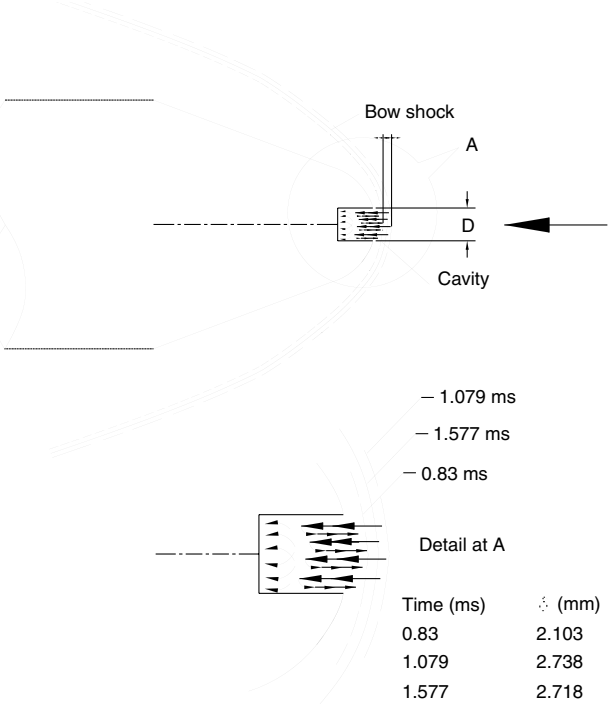

Fig. 7 Schematic representation of the flowfield features around the missile body with a forward-facing cavity.

The above phenomena can be explained in the schematic diagram of a cavity flowfield, shown in Fig. 7. It clearly signifies that the shock standoff distance oscillates for a cavity model. There is a significant increase in the shock standoff distance (approximately 29%) when the time interval changes from 0.830 to 1.577 ms, which clearly signifies that the location of a shock wave is not stationary for a cavity model. The overall comparison of shock angle and shock standoff distance for different configurations obtained from experiments and theory is shown in Table 2. The experimentally measured shock angles match well with the theoretical expression [24]. Because a steady-state flow condition is assumed in the numerical simulation, we would not be able to observe the time-accurate bow-shock motion in postprocessing of CFD. However, bow-shock motion and shock standoff distance are visualized from the experimental results of the schlieren image. Indeed, a steady flow state is used to an extent to determine the peak and surface heat transfer rate of a test model. These results also ascertain the quality of the hypersonic flow in the tunnel test section and demonstrate the applicability of this flow visualization technique to a cavity in hypersonic flowfields.

C. Heat Transfer Measurements

Platinum thin-film sensors were used to measure the heat flux on the surface of test model. These sensors are made in-house, and development of platinum thin-film heat transfer gauges are done by using a planar magnetron sputtering technique. Sensors deposited on the ceramic glass (Macor) inserts, which are embedded in the metallic model, are used to measure the surface convective heat transfer rates. The sensors are typically designed so that the thickness of the sensing element is much less than that of the substrate. Hence, the sensing element has an almost negligible effect on the heat

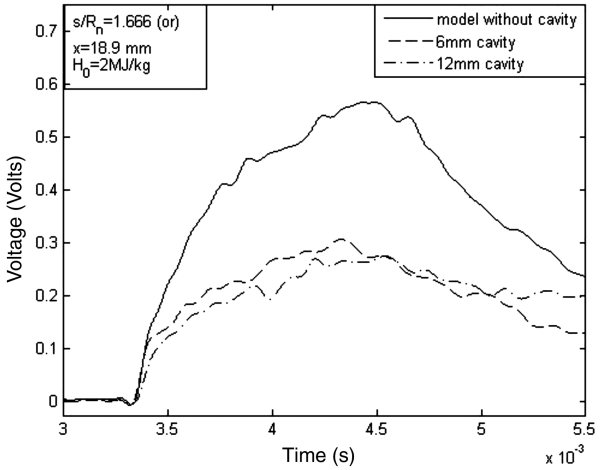

Fig. 8 Typical temperature–time history from platinum thin-film sensors.

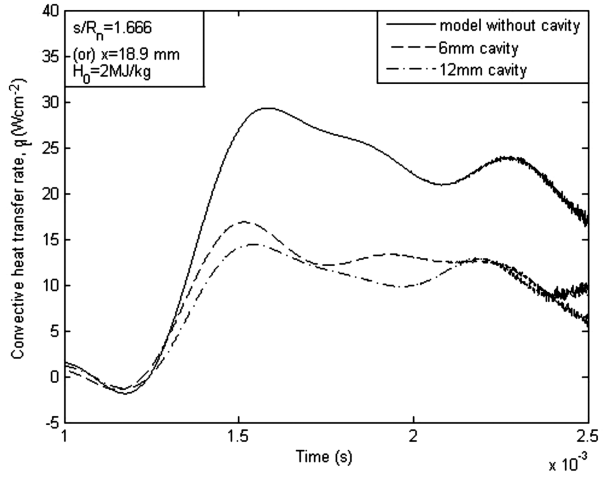

Fig. 9 Numerically integrated heat transfer signal for platinum thin-film sensors.

transfer rate to the substrate, and the temperature measured by the sensing element is identical to the temperature at the surface of the substrate. Moreover, it is very important to ensure a minimum thickness of Macor [25] for a given test model, so that the classical 1-D semi-infinite slab heat transfer model usually used for calculating the surface heat transfer rates is valid. The sensor is powered using a constant current power supply (∼20 mA), through which it is connected to a National Instrument data acquisition system. The initial resistance of these passive gauges is maintained at around 30 Ohms. The change in resistance of the gauge due to change in temperature gives a change in voltage across the gauge with respect to time, which corresponds to the temperature–time history at the gauge location on the model surface. With the calibration curve of the temperature coefficient of resistance of thin film and thin-film backing material property, the convective surface heat transfer rates can be determined by numerical integration [26] of temperature–time history signals.

Table 2 Comparison of shock standoff distance and shock angle for a missile shaped body, flying at Mach 8

		Experiment	Theory		Experiment	Theory
Blunt cone without cavity	Δ, mm	1.705	2.212	θ, deg	26.8	27
6 mm cavity		2.32			24.6	
12 mm cavity		2.59			24.3	

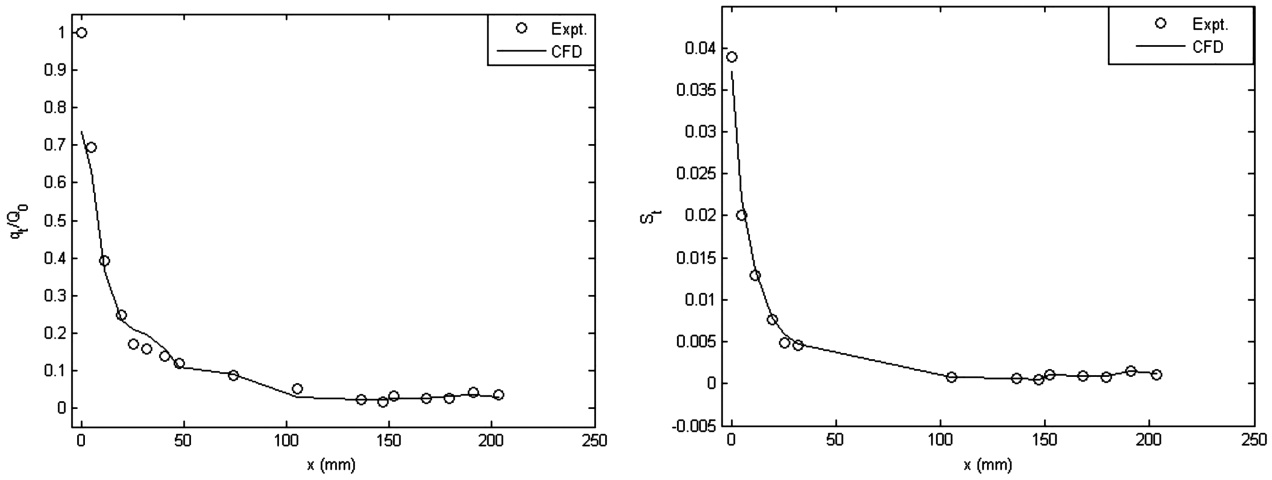

a) b)

Fig. 10 Variation of convective heat transfer rates over the surface of the 41 deg apex-angle missile-shaped model at 0 deg angle of attack and a freestream Mach number of 8 showing the a) normalized heat transfer rate and b) Stanton number, where Expt. stands for experiment.

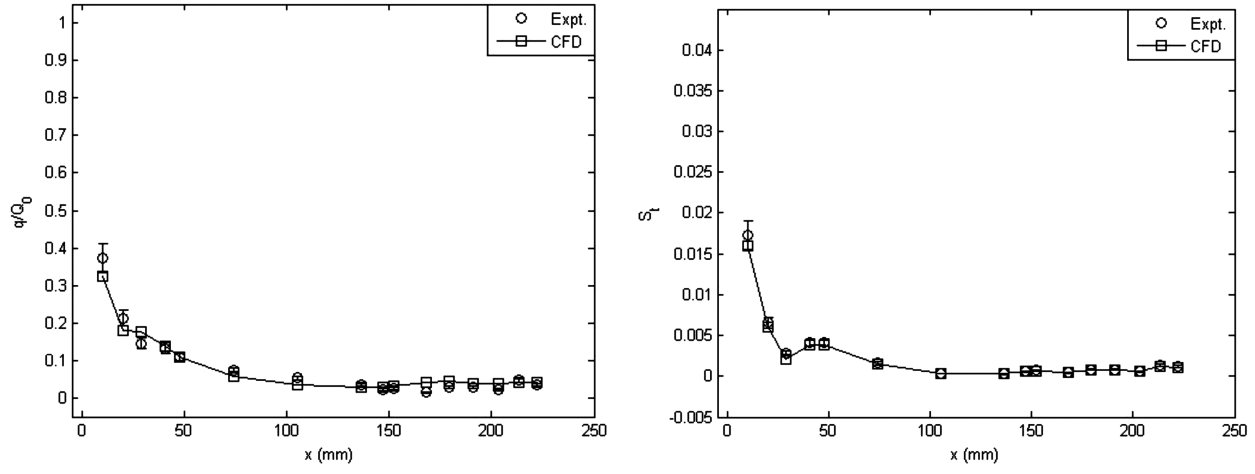

a) b)

Fig. 11 Variation of convective surface heat transfer rates over the surface of a missile-shaped model with a 6 mm cavity at 0 deg angle of attack flying at a freestream Mach number of 8 showing the a) normalized heat transfer rate and b) Stanton number.

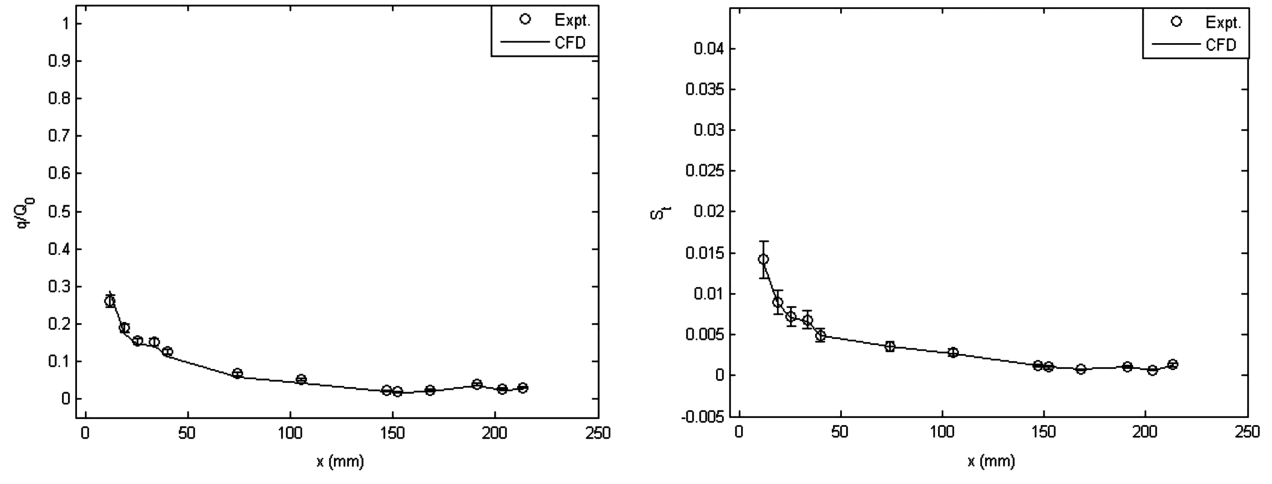

a) b)

Fig. 12 Variation of convective surface heat transfer rates over the surface of a missile-shaped model with a 12 mm cavity at 0 deg angle of attack flying at a freestream Mach number of 8 showing the a) normalized heat transfer rate and b) Stanton number.

The typical surface temperature (voltage-time trace) recorded by the thin-film gauge during the experiment is shown in Fig. 8 for a model without and with cavity configurations. The parabolic portion of the signal (without cavity configuration) is selected for the numerical evaluation of heat flux because this portion of the signal represents the steady/constant heat flux to the body, and the signal for a cavity model is not of a perfect parabolic shape, which is a clear indication of the flow being unsteady in that region. The corresponding numerically obtained typical heat transfer signals are shown in Fig. 9. The measured experimental results of normalized heat transfer rate (q_t/Q_0) and Stanton number (St) over the surface of a missile model without a cavity and with 6 and 12 mm cavities flying at Mach 8 are shown in Figs. 10–12. In these figures, Q_0 is the stagnation-point heat transfer rate, and it is obtained from a model without a cavity (Fig. 1a) mounted at zero degree angle of attack. The computed values of heat transfer rates have been plotted in the corresponding figures in order to have a better comparison between the measured and numerical data. Considerable differences can be seen between these two values, and the difference may be due to unsteady oscillations in the flowfield and the assumption of laminar flow boundary conditions. However, in the region of the frustum it has been found that the experimental results match very well with computed results.

Stanton number based on the tunnel freestream conditions, is given by the expression

$$St = \frac{q(t)}{[\rho_\infty V_\infty (H_0 - H_w)]} \tag{1}$$

The predicted maximum possible heating rate occurs near the stagnation zone of the model, and beyond the maximum heating point (stagnation point) the measured heating rates decreased gradually, as seen in Fig. 10. By adding the cavity diameters of 6 and 12 mm, the reduction in heat transfer can be clearly seen, and it is evident from Figs. 10–12 that the preceding single phenomena has been observed for cavity configurations near the stagnation zone. The measured data and CFD prediction using a Navier–Stokes solution agree within about ±15% until the corner of the conical frustum. At an axial location of 105.1 mm (i.e., from the stagnation point), the heating rate was nearly constant, which is clearly seen from CFD simulation. Then, it decreases rapidly before reaching a minimum value (i.e., 5 to 10% of stagnation heating rate).

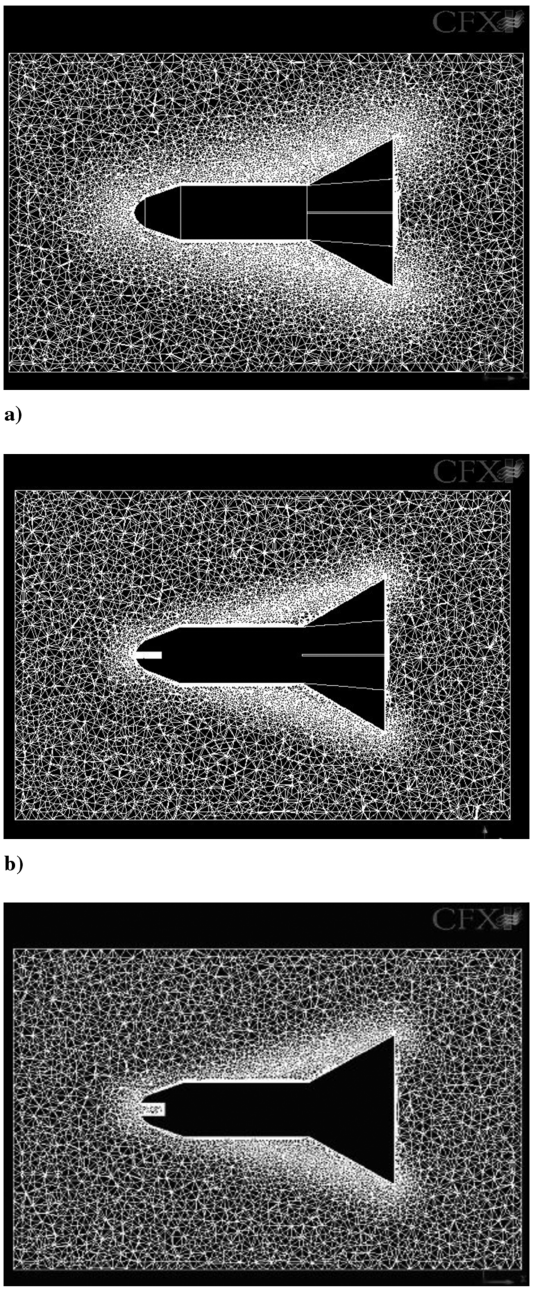

Fig. 13 The typical grid used in the numerical simulation of flowfields around a missile-shaped body a) without a forward-facing cavity, b) a 6 mm cavity, and c) a 12 mm cavity.

D. Description of "Cooling" Mechanism

Recent experiments with cavities showed a reduction in temperature in the vicinity of the cavity lip due to the presence of a cool ring [16,19,27]. A forward-facing cavity at hypersonic Mach numbers has oscillating pressure levels within a cavity, which is one of the dominant experimental flow features. However, a deep cavity has been provided for both the configurations to obtain resonant oscillation. It has been noticed that the heat transfer measurement for cavity configuration shows a temperature that is less than that of similar steady flow where no oscillations are present. Strong longitudinal pressure oscillations within the cavity correspond to strong longitudinal oscillations of the bow-shock position. Typically the position of bow shock oscillates sinusoidally between two positions: one is close to the cavity mouth and the other is relatively far upstream. When the bow shock is moving towards the cavity mouth, the relative shock Mach number and the stagnation temperature of the inflow air reduces, and although the bow shock is moving upstream, it increases the relative shock Mach number and the stagnation temperature of the inflow air. However, this hot air is converted away from the nose-tip region. Note that the air temperatures just downstream of the bow shock are much lower during the movement of bow shock towards the cavity mouth. The flow also separates and forms a recirculation region, which protects

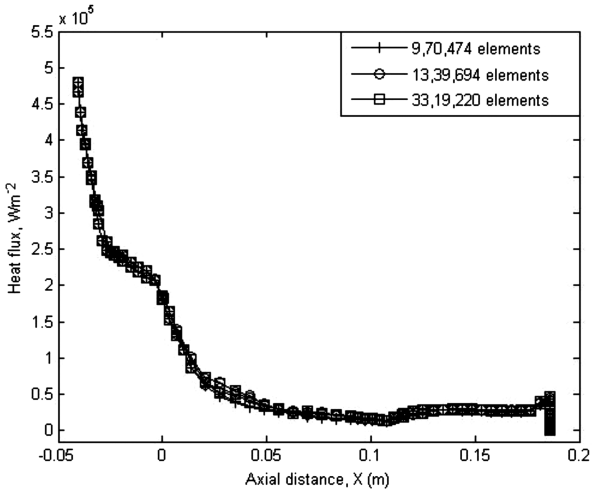

Fig. 14 Assessment of grid resolution study (i.e., mesh convergence) for a missile-shaped body without a cavity.

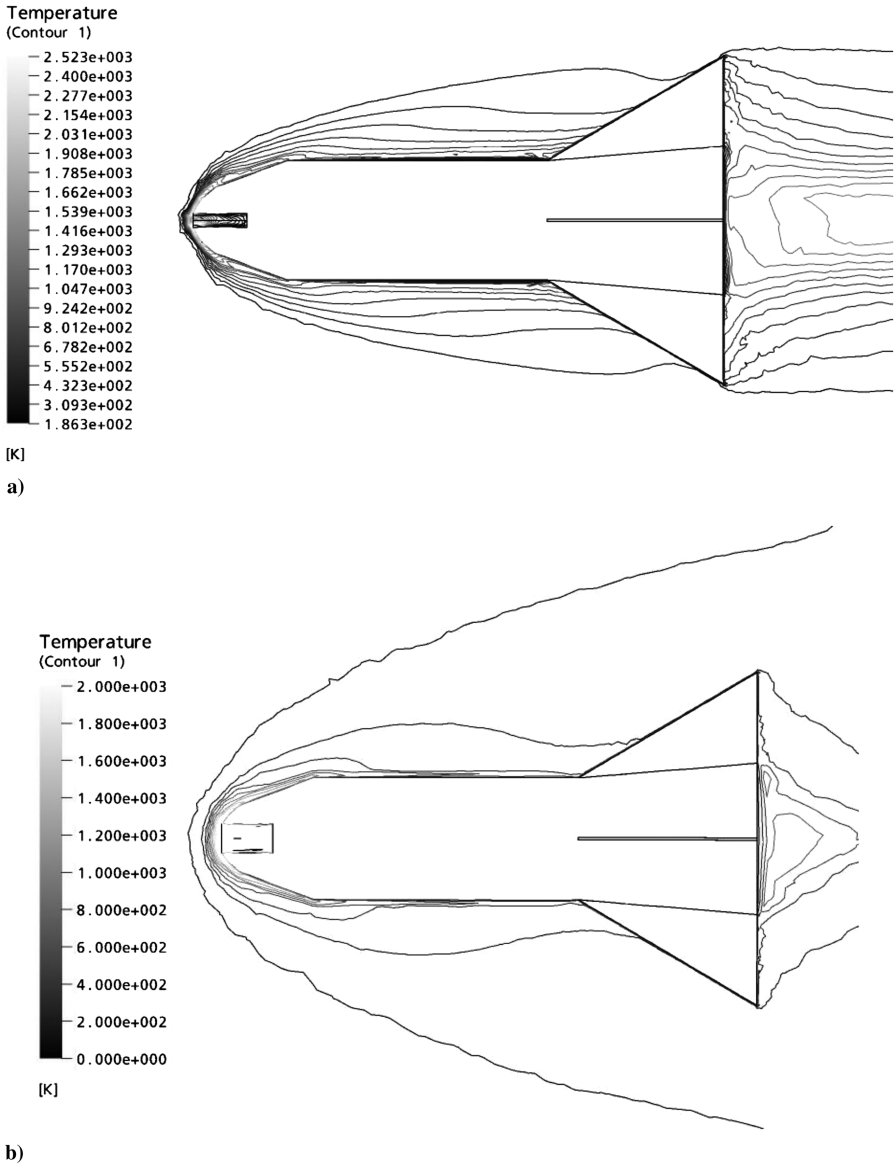

Fig. 15 Computed temperature distribution over a missile-shaped body flying at Mach 8 with a forward-facing cavity of a) 6 mm and b) 12 mm diameter.

the outer surface from the extremely hot gas convecting away from the nose region. Consequently, the oscillating forward-facing cavity flow reduces the mean stagnation temperature of the flow in the vicinity of the nose tip and results in net reduction in surface heating, and, hence, dramatic bow-shock motion (i.e., large mean bow-shock speed) occurs to produce a substantial "cooling" effect. The shock wave movement is observed in the schlieren photograph (Fig. 6), and, indeed, it indicates an erratic and violent motion (Figs. 6 and 7) and the shape of the shock wave changes (Fig. 6). Yuceil and Dolling [5] and Engblom et al [19] adopted a cavity with an L/D ratio of 1.19 to 1.23 to measure the IR image and pressure signals at the cavity base. Silton and Goldstein [16] carried out an investigation (with L, D, and lip radius) to determine the cavity geometry that would delay the ablation onset. They have not investigated the variation of aerodynamic forces and shock standoff distance except to determine the heat transfer rate. The preliminary investigation of the current

Fig. 16 The photographic view of newly designed three-component balance system.

study is to understand the cooling mechanism and to measure how aerodynamic forces that will be affected by the presence of a cavity (L/D of 2 to 4).

In this investigation commercially available robust fluid engineering software called CFX-Ansys 5.7 has been used to simulate the flow fields around a missile-shaped body with various configurations flying at a hypersonic Mach number of eight for complementing the experimental values of aerodynamic coefficients and heat transfer rates obtained over the body in a hypersonic shock tunnel. This software package provides numerical solutions to the compressible 3-D Navier–Stokes equations. The computations are carried out with various angles of incidence. It is a complete Navier–Stokes solver in which both steady and unsteady flow problems can be solved using both stationary and rotating frames of reference. It has good grid-generating capabilities like nonorthogonal, curvilinear, and multiblock grids with embedded grid refinement utilities. It uses state-of-the-art computational fluid methodology by combining the advantages of both the finite element and finite difference methods. Thus, the code combines the geometrical information of the finite element techniques with the simplicity of the finite difference techniques. Because the complex geometries are handled by finite element methodology whereas the solutions are obtained by finite difference analogs, the method yields rapid and accurate solutions to flows around complex boundaries. In the present investigation, second-order accurate schemes are used and a numerical study has been carried out for a steady-state flow condition.

The various boundary conditions used in this simulation are based on the experimental freestream conditions obtained in the shock tunnel test section, which are as follows:

1) *Inlet*: At this boundary of the computational domain, the velocity, static pressure, and static temperature of the flow have been specified. Typical values used here are velocity $V = 1908$ m/s, pressure $= 205$ Pa, and temperature $= 143$ K for a flow Mach number of eight. These are the flow properties obtained for an enthalpy level of 2 MJ/kg.

2) *Outlet*: At the outlet of the computational domain, all variables are extrapolated from the interior domain.

3) *Wall*: The wall boundary condition is used at the missile model surfaces and the fluid at these surfaces is assumed to have a no-slip condition. A constant temperature of 300 K is specified at the walls.

4) *Symmetry*: Other bounds of the computational domain, excluding the inlet and outlet, are specified as symmetry planes. The fluid velocity is assumed to be tangential at these symmetry planes.

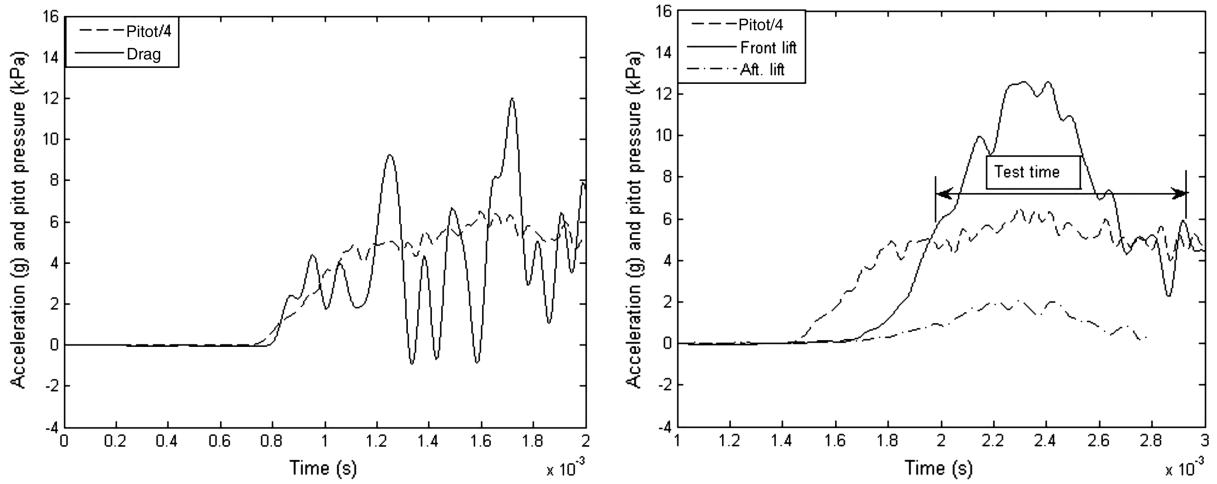

a) b)

Fig. 17 Typical signals from various accelerometers mounted in the model and accelerometer balance system for the missile-shaped body flying at Mach 8.

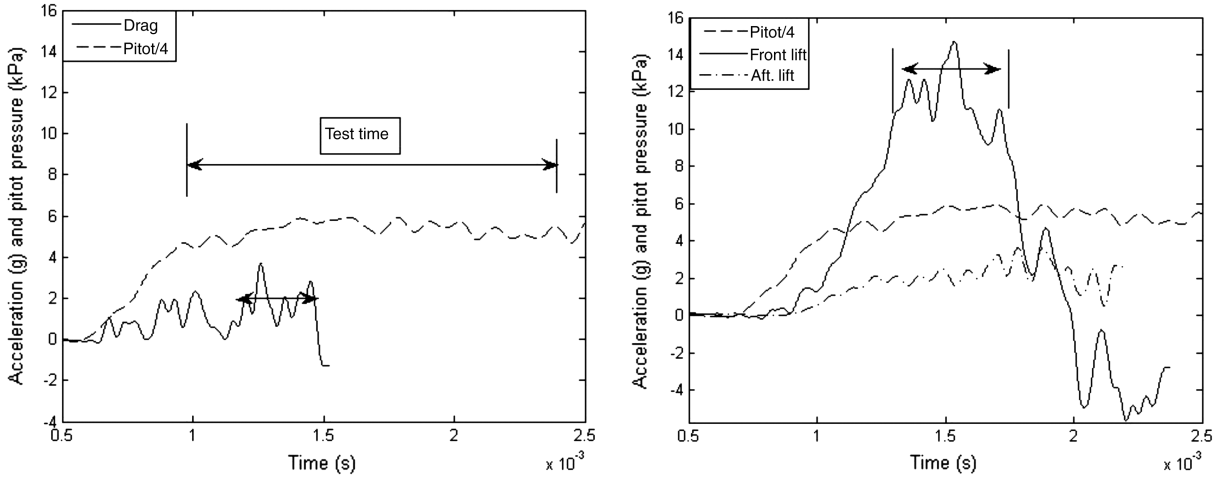

a) b)

Fig. 18 Typical signals from various accelerometers mounted in the model and accelerometer balance system for the missile-shaped body mounted with a 6 mm cavity flying at Mach 8.

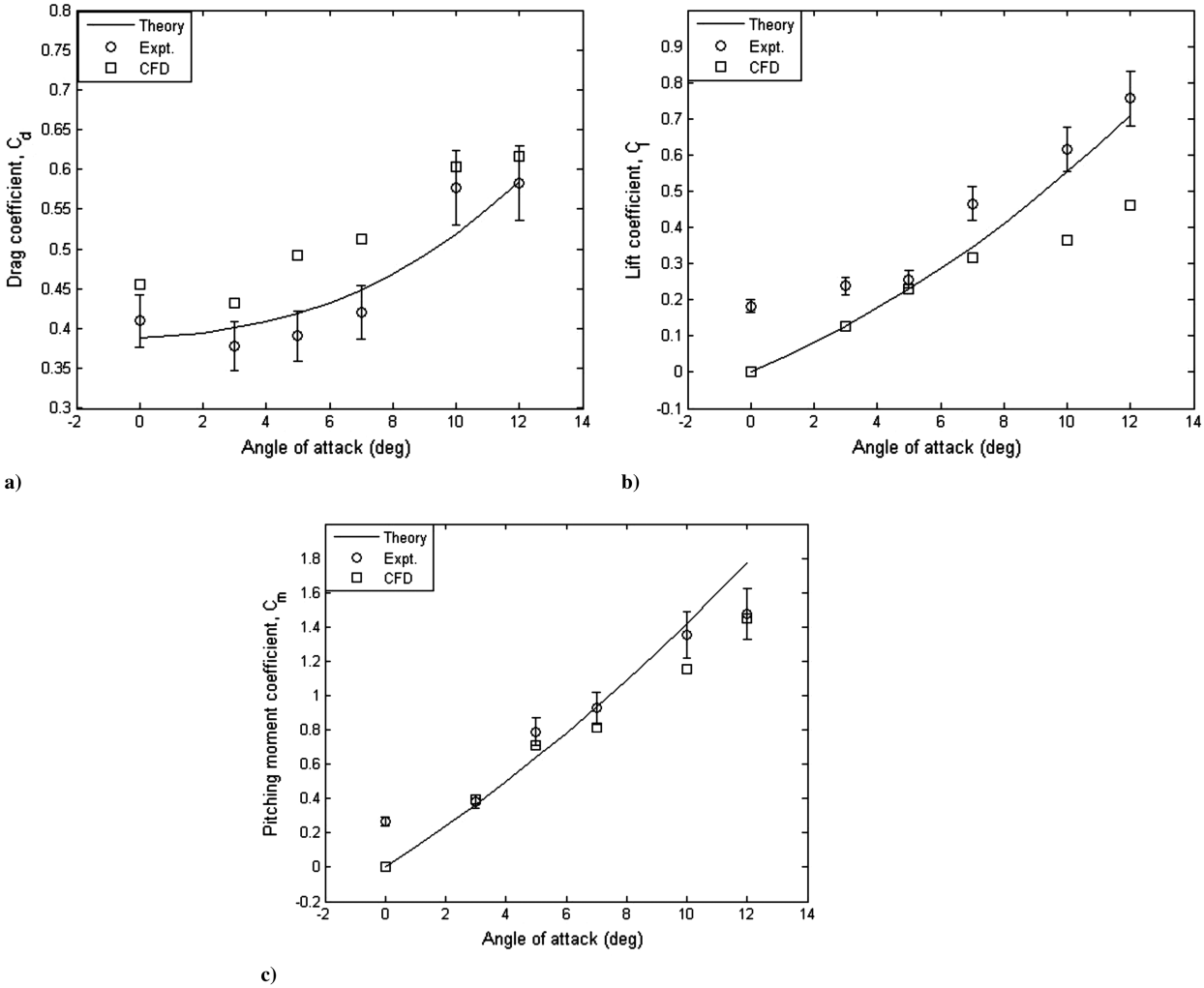

Fig. 19 Variation of aerodynamic coefficients for the 41 deg apex angle of a missile model with a blunt cone at Mach 8 for various angles of attack showing the a) drag coefficient, b) lift coefficient, and c) pitching moment coefficient.

A typical grid used for the computation of the flowfield around the missile model without and with forward-facing cavities is shown in Fig. 13. In the initial simulation, the multiblock, body-fitted grid used for the computations (Fig. 13a) has a total number of around 2,13,848 nodes, 8,31,269 tetra hedra, and 9,67,835 elements. The chosen mesh is hybrid with both triangular prisms near the model surface (structured mesh) and tetrahedron mesh for the remaining flow domain (unstructured mesh). Tetrahedron cell spacing is used for a typical grid used in the present investigation. The number of grid points has been increased (i.e., grid resolution study) in the subsequent runs, and simulations are once again carried out to check the variations in heat transfer rates. A high-resolution second-order accurate scheme has been used for the computations with a local time step of 0.8. The target residuals to terminate the simulation have been set at 1.0×10^{-5}. About 1500 iterations (time steps) have been used for the convergence, and approximately 4 h of CPU time were required for the simulation on an Intel Pentium 4, 2.8 GHz processor and 1 GB of RAM speed. The program was run on a Windows NT platform.

Figure 14 shows the surface heat transfer rate predicted by three different meshes and zero on the X-axis refers to the junction of the blunt cone and cylinder-frustum-fin configuration. It is seen that there is no change in the heat transfer rate, irrespective of grid size. These meshes produce very close matching throughout the model length. Finally, total number of around 13, 39,634 nodes (grid points) have been chosen for the present study.

In numerical computations the focus is only on the stagnation region of the model. The typical distribution of temperature over the test model (with cavity) at Mach 8 is shown in Fig. 15. The reductions in the heat transfer rate are dramatic. The temperature indicates a large variation in the cavity and near the cavity zone (Fig. 15). Temperature is quite uniform upstream of the cavity. Localized surface heating can be seen near the cavity, which is due to the presence of a vortex structure in the flow. The maximum heating for both the cavity configurations occurs inside the cavity, where the flow is usually decelerated and brings it down to zero velocity. In this region, boundary layers are very thin. This is also verified by the experimental measurements.

E. Drag Measurements

During reentry, the vehicle undergoes severe heating, aerodynamic drag, difficulties in stability control, and structural constraints are some of the major issues involved in design of any hypersonic vehicle. To eliminate the problems highlighted previously, a novel method of a forward-facing cavity has been used in the present investigation to reduce the heat transfer rate and aerodynamic drag. Although, the nose-cavity geometry occupies only a small region in the nose tip, the effect on the drag is still of importance.

The newly designed three-component balance system is used to measure fundamental components of aerodynamic forces and moments, namely lift, drag, and pitching moment, on a generic hypersonic missile model configuration as shown in Fig. 16. It consists of three accelerometers, of which two are mounted on the balance system to measure the lift force and other is mounted along the axis of the model to measure the drag force. These accelerometers are rigidly attached to the inside wall of the hallow model, which in turn is attached to a central sting using two rubber bushes. These two

rubber bushes act as lift springs while in compression or tension and both act as drag springs in shear, thus forming a flexible suspension system in conjunction with the central fastening sting. The lift force accelerometers are mounted onto the metallic arms of the balance, as shown in Fig. 16. The balance system measures simultaneously the acceleration experienced by the body in two normal directions (X and Y). Although not reported here, exhaustive measurements have been carried out (i.e., keeping yaw and roll angles to be 0 deg) on side force, yawing, and rolling moments, for a missile-shaped body fitted with different cavity diameters in order to understand the flowfield features. These studies have shown that the aerodynamic loads of side force, yawing, and rolling moments are very small, and, hence, the present set of experiments has been focused on the measurement of fundamental aerodynamic forces. Therefore, the magnitude of lift and drag signals is very crucial to estimate the lift-to-drag ratio of a missile model with a cavity.

During the short run times encountered in the shock tunnel, the model along with the accelerometers moves as a free body, and the resulting accelerations are measured from the outputs of the corresponding accelerometers (drag and lift). These accelerometers, having 12 mm height and 7 mm diameter, are supplied by PCB-Piezotronics, Ltd. (model M303A). An accelerometer with the frequency range of 10 kHz was used in the present balance system. The accelerometer output was assumed to be linear with the applied acceleration over the range up to 500 g. Most of the time, the calibration constant supplied by the company will be quite accurate, but it is advisable to calibrate the piezo crystal accelerometers before the experiments, because harsh environmental changes and temperature variations will produce drifts in the sensitivity of accelerometers. A negligible difference has been found between the sensitivity values obtained from the calibration and the sensitivities given by the manufacturer. Hence, for the present study, the accelerometers are calibrated and sensitivity ranges from 8.45 to 10.15 mV/g.

The normal force $N(t)$, center of pressure location from base of the model (e_N), and axial force $C(t)$ on the model are calculated using the measured accelerations from the following equations [28]:

$$N(t) = m\frac{b'\xi_{N1} + a'\xi_{N2}}{a' + b'} \tag{2}$$

$$e_N = \frac{I}{m}\frac{(\xi_{N1} - \xi_{N2})}{b'\xi_{N1} + a'\xi_{N2}} \tag{3}$$

$$C(t) = m\xi_A \tag{4}$$

Knowing the angle of attack and the center of pressure location from the base of the model, the fundamental aerodynamic coefficients can be computed by using the following equations:

$$C_l = (N(t)/(q_\infty S))\cos\alpha - (C(t)/(q_\infty S))\sin\alpha \tag{5}$$

$$C_m = \left(\frac{N(t)}{q_\infty s}\right)\left(\frac{\{(X_{c.g})_{\text{base}} + e_N\}}{D_B}\right) \tag{6}$$

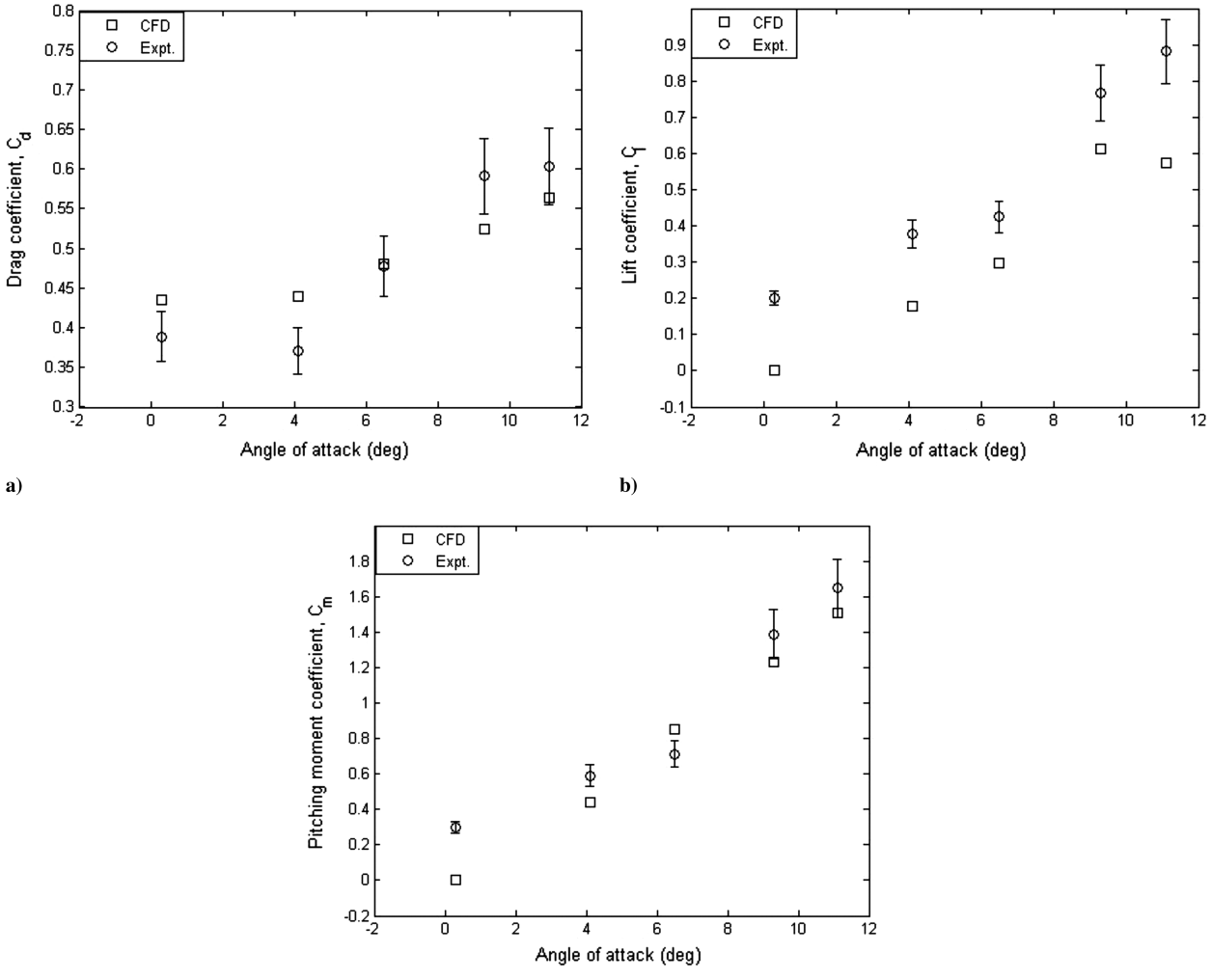

Fig. 20 Variation of aerodynamic coefficients for the missile body with a 6 mm cavity flying at Mach 8 for various angles of attack showing the a) drag, b) lift, and c) pitching moment coefficient.

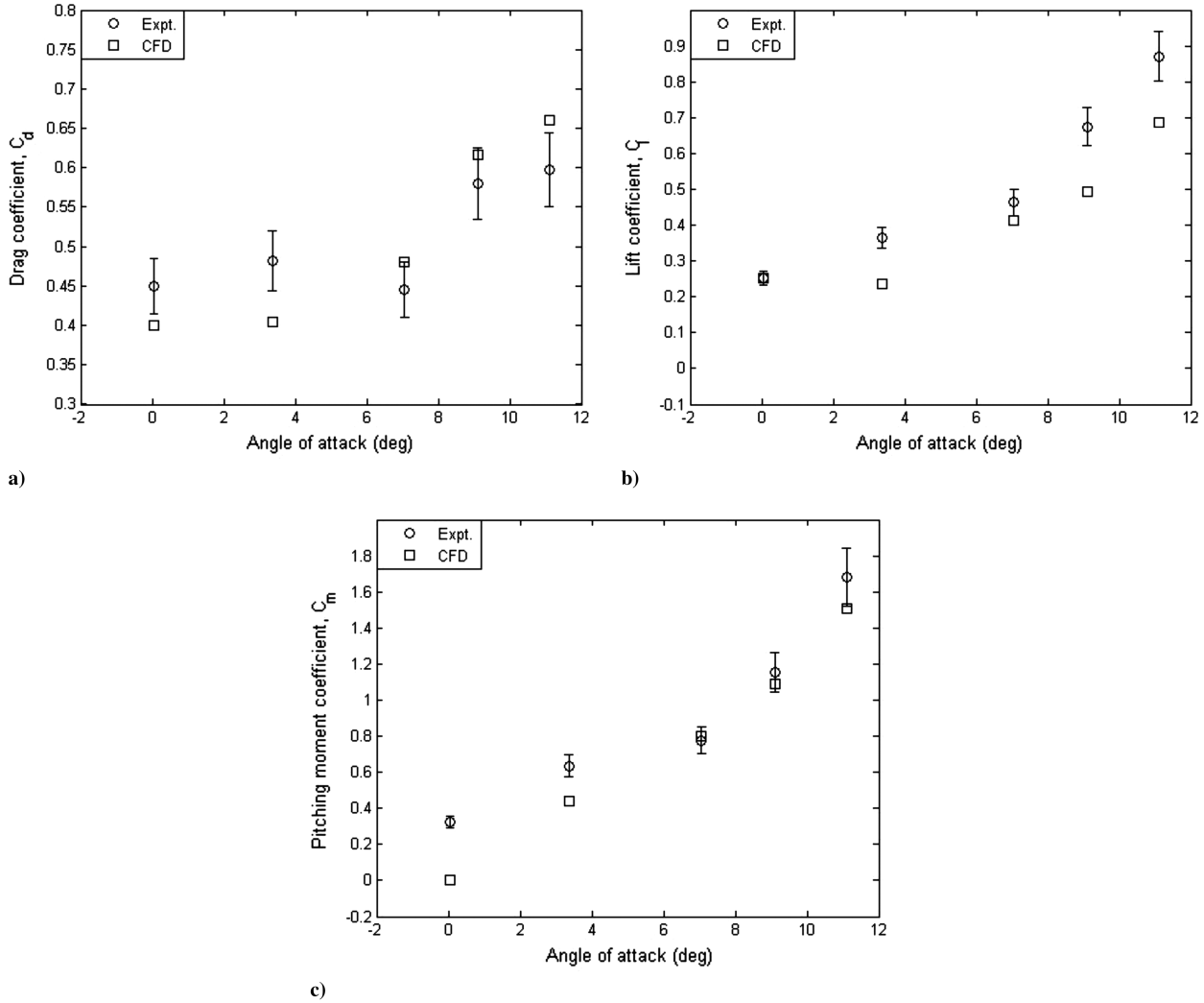

Fig. 21 Variation of aerodynamic coefficients for the missile body with a 12 mm cavity flying at Mach 8 for various angles of attack, including a) drag, b) lift, and c) pitching moment coefficient.

$$Cd = (C(t)/(q_\infty S))\cos\alpha + (N(t)/(q_\infty S))\sin\alpha \qquad (7)$$

The typical recoded outputs from the accelerometer balance system for the missile-shaped model without a cavity flying at Mach 8 are plotted in Fig. 17. A pitot signal (pressure-history) obtained in the test section is superimposed on the measured accelerometer signals (i.e., for a missile-shaped body without a cavity flying at Mach 8), which indicates the steady flow test time during the shock tunnel testing. Indeed, the data reductions of force and moment components are made much simpler by inferring the steady test time from the pitot signal. However, high-frequency noise is seen from Fig. 17a, and this irregular high-frequency noise in the case of the baseline may be due to the impact of either the particle (i.e., primary diaphragm) or paper diaphragm on the surface of the nose cone (where the drag accelerometer is mounted to measure the acceleration).

Drag reduction is one of the important objectives for the present investigation, and it can usually be obtained through large-scale flowfield modifications upstream of the blunt body. Techniques such as highly localized perturbations, including energy, force, mass, and structural perturbations within the upstream flow, are usually adopted to modify the flowfield. Introducing a forward-facing cavity in the nose region of hypersonic vehicle is shown to be very effective in reducing the peak heat without modifying the flowfield.

Hence, measurements have been repeated for cavity configurations, namely 6 and 12 mm, respectively, and the signals obtained from the accelerometer balance system for a 6 mm cavity are shown in Fig. 18. It is evident that the steady state of 600 μs was seen from the responses of lift accelerometers. However, the drag signal contains irregular and high-frequency noise, which is due to the presence of the forward-facing cavity. Hence, the method of deconvolution [29] has been used here to infer the drag force, and it was found that a good recovery can be achieved.

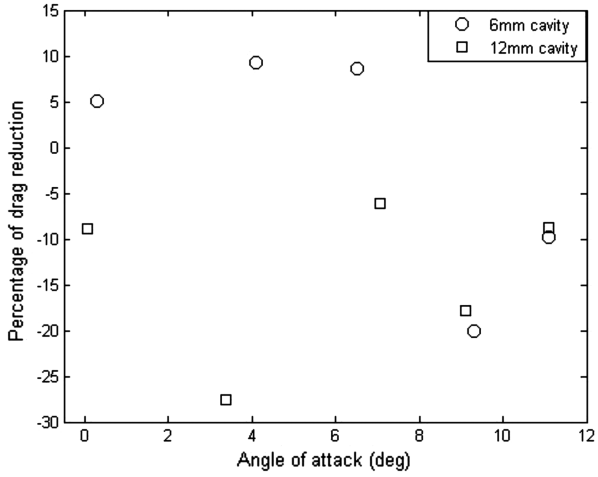

Fig. 22 Variation of the percentage of the drag reduction with an angle of attack for the forward-facing cavity missile-shaped body flying at Mach 8.

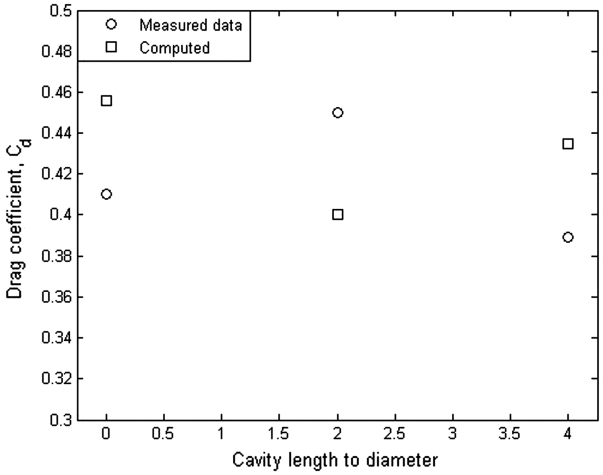

Fig. 23 Variation of the drag coefficient for a missile-shaped body with a forward-facing cavity at two different L/D.

The measured value of the drag coefficient for different angles of attack for a missile-shaped body is shown in Fig. 19. Similarly the theoretical and numerical results are also plotted, and it was found that the measured fundamental aerodynamic coefficient matches well with the theory at moderate angles of attack and shows slight deviation at both lower and upper angles of attack. The measured drag and pitching moment show $\pm 10\%$ and $\pm 24.2\%$ deviation, respectively, from the value predicted by theory. The measured values for 0 deg angle of attack is about 26% higher than predicted lift coefficient. The measured drag coefficient for the missile-shaped body with forward-facing cavities, namely 6 and 12 mm at various angles of attack, are shown in Figs. 20 and 21. Cavity studies show that the drag coefficient increased as both cavity diameter (D) and angle of attack increased.

The cavity configuration with a L/D ratio of 4 (i.e., 6 mm cavity) results in approximately 5.12% drag reduction at zero angle of incidence whereas with an L/D ratio of 2, an 8.88% increase in aerodynamic drag is observed. The smaller cavity pushes the body shock away from the cavity mouth at lower angles of attack and, hence, the region of low pressure and temperature exists, whereas for

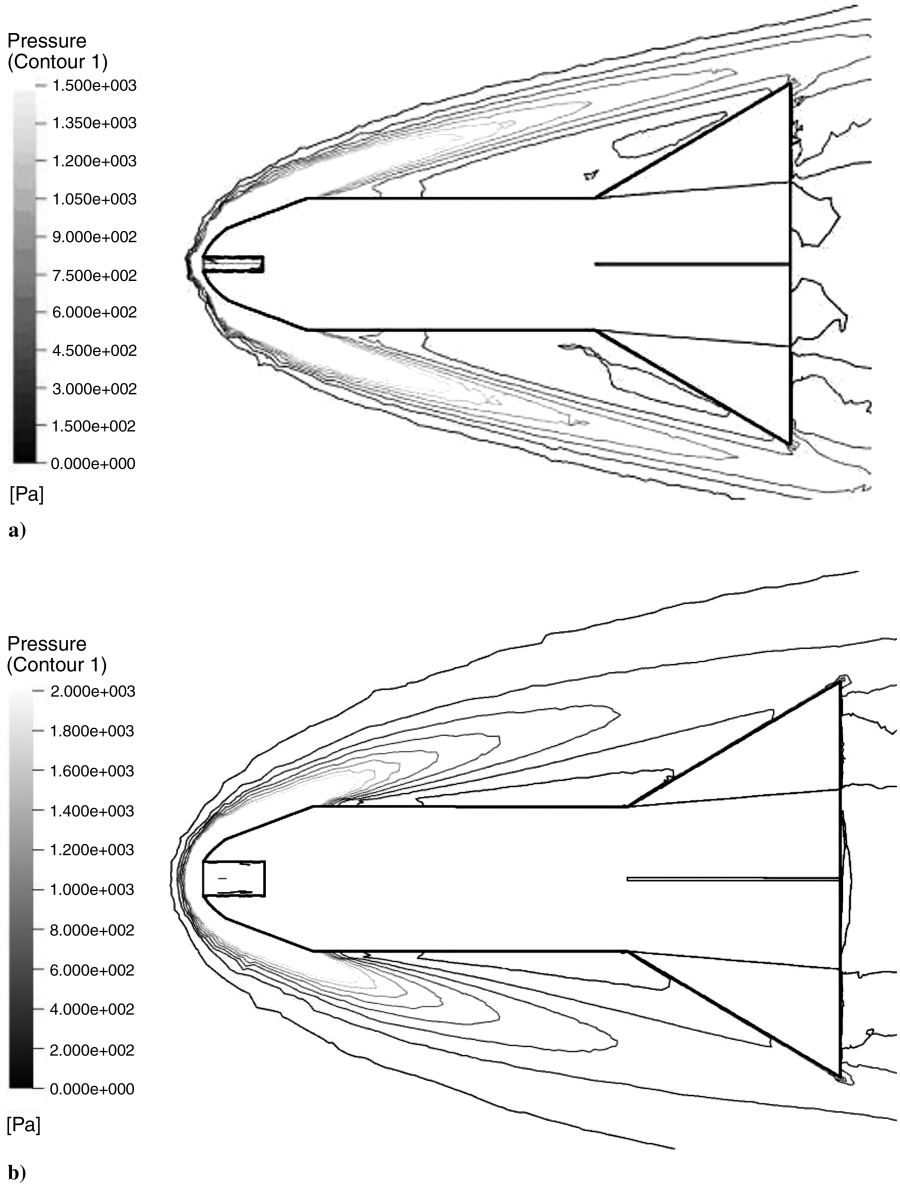

Fig. 24 Computed pressure distribution over a missile-shaped body flying at Mach 8 with a forward-facing cavity of a) 6 mm and b) 12 mm diameter.

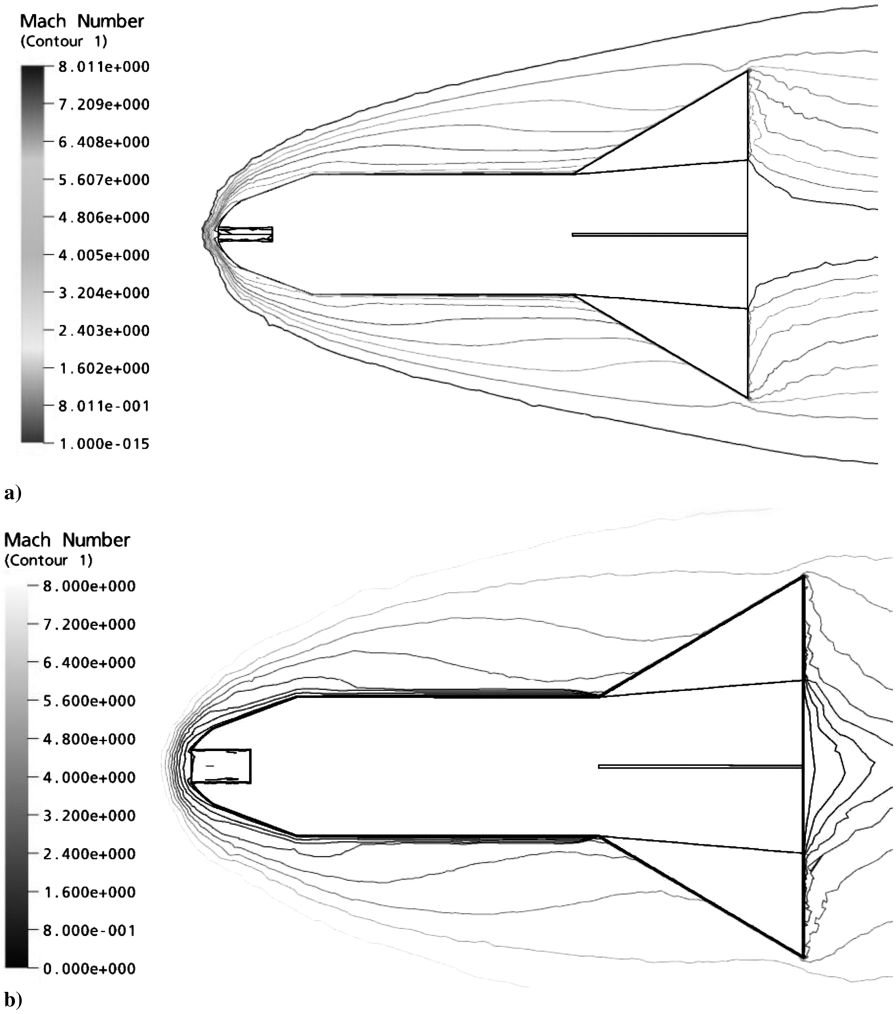

Fig. 25 Computed Mach number distribution over a missile-shaped body flying at Mach 8 with a forward-facing cavity of a) 6 mm and b) 12 mm diameter.

a 12 mm cavity, the shock is oscillating violently about the cavity. However, both the cavity configurations exhibit the increase in drag coefficient with an increase in angle of attack. Because of the unsteady oscillation present in the both cavity configuration, variation in drag coefficients are observed between the experiment and computation. This is indicated by the scatter in the measured drag coefficient especially at moderate angles of incidence, as seen in Figs. 20 and 21. In addition, an unsteady flow solver has not been used for the computation, which may have a direct impact on the accuracy/uncertainty of the CFD simulation.

The variation of percentage of drag reduction with respect to angle of attack for a missile model with different cavity diameters is shown in Fig. 22. It is clear that about 9.2% drag reduction is observed for lower angles of attack (up to 6.5 deg) with a 6 mm cavity, whereas at higher angles of attack, it shows an increase in aerodynamic drag. With a 12 mm cavity, the drag coefficient increases at all angles of attack. In addition, the effect of the diameter of the cavity on the drag reduction was also investigated, and these results are presented in Fig. 23. The computational results are also plotted here, and it was found that the difference is about 11% between the measured data and computational analysis.

The typical distributions of pressure over the test model (with cavity) at Mach 8 are shown in Fig. 24. Depending on both the cavity shape and length-to-diameter ratio, shock wave structures are modified significantly, and as a result pressure drag is reduced. Pressure is quite uniform upstream of the cavity, which is very similar to temperature variation. The pressure distribution plot (Fig. 24) shows a strong bow shock in front of the cavity, and in the cavity there are also pressure variations, which are associated with the flow of the vortex structure. In addition, in front of the cavity, the pressure is quite uniform and equivalent to its freestream values. The impact of the cavity plays a vital role in flowfield structure. The maximum pressure experienced near the nose portion of 6 mm cavity is 1500 Pa and that for 12 mm cavity is 2000 Pa, which clearly shows that the 6 mm cavity has less aerodynamic coefficient compared with the 12 mm configuration.

In the cavity, the flow is oscillatory and the produced shock waves are unsteady in nature. From the above contour plots, the dominant physics of the flow oscillation can be seen very clearly, and the current numerical simulation seems to capture features of the flowfield in the presence of the cavity. Figure 25 shows the Mach number distribution pattern for two different cavities, and large vortical structures can be seen from the contour plot.

F. Measurement Uncertainties

The uncertainty analysis [30] has been carried out, based on the uncertainties associated with the gauge characteristics, circuitry, data acquisition system, calibration, and data reduction techniques. The measured values of heat transfer rates are believed to be accurate to $\pm 6.08\%$ whereas the uncertainties associated with Stanton number and correlated Stanton number are 16% with helium as the driver gas. Various factors, such as discontinuity in substrate and departure from one-dimensional heat conduction during the run time, contribute to the uncertainties in the measured Stanton number. The estimated uncertainties in the measured data are $(\Delta C_d/C_d) = \pm 0.0783$,

$(\Delta C_l/C_l) = \pm 0.0806$, and $(\Delta C_m/C_m) = \pm 0.0953$. Uncertainties in the sensor sensitivities, setting of the angle of attack, freestream conditions in the tunnel test section, the restraint offered by the rubber bushes to the free flight of the model during test time, outputs of the accelerometer balance system, and data acquisition systems are some of the factors that contribute to the preceding force measurement uncertainties.

IV. Conclusions

In general, this technique is useful in modifying the flowfield and weakening the shock structure associated with the blunt body. The structure of the hypersonic flow over a cavity has been studied experimentally and numerically and can be used as local surface heating reduction devices. Experimental data compare reasonably well with numerical predictions from a Navier–Stokes solver. Detailed discussions of the bow-shock behavior associated with two different cavities at a freestream Mach number of 8 are presented. For each of the tests performed with a cavity, the bow shock is oscillated during the test. The mean shock standoff distance was shown to be dependent of cavity diameter.

The net reduction of 35 to 40% in surface convective heating transfer rates has been observed for cavity configurations near the stagnation zone at 0 deg angle of attack. Cavity configuration with an L/D ratio of four (i.e., 6 mm cavity) results in approximately 5% drag reduction at zero angle of incidence. With an L/D ratio of 2, 10% increase in aerodynamic drag is observed. The addition of a cavity (i.e., smaller diameter) resulted in a slight increase in the missile L/D ratio, and it increases at higher angles of attack for both cavity configurations. The fluctuations in the measured heat transfer rates indicate the oscillatory behavior of the flow.

In the present investigation, the analysis has been carried out only for laminar flow, and it was found that the effect of changing the cavity length-to-diameter ratio ($L/D = 2$ and 4) is rather small. It may be considerably greater for the transitional flow compared with the laminar flow.

References

[1] Menezes, V., Saravanan, S., Jagadeesh, G., and Reddy, K. P. J., "Experimental Investigations of Hypersonic Flow over Highly Blunted Cones with Aerospikes," *AIAA Journal*, Vol. 41, No. 10, 2003, pp 1955–1966. doi:10.2514/2.1885

[2] Satheesh, K., and Jagadeesh, G., "Effect of Concentrated Energy Deposition on the Aerodynamic Drag of a Blunt Body in Hypersonic Flow," *Physics of Fluids*, Vol. 19, No. 3, March 2007, pp. 1–4.

[3] Sahoo, N., Kulkarni, V., Saravanan, S., Jagadeesh, G., and Reddy, K. P. J., "Film Cooling Effectiveness on a Large Angle Blunt Cone Flying at Hypersonic Speed," *Physics of Fluids*, Vol. 17, No. 3, March 2005, pp. 1–11. doi:10.1063/1.1862261

[4] Huebner, L. D., and Utreja, L. R., "Mach 10 Bow-Shock Behavior of Forward-Facing Nose Cavity," *Journal of Spacecraft and Rockets*, Vol. 30, No. 3, 1993, pp. 291–297. doi:10.2514/3.25513

[5] Yuceil, B., and Dolling, D. S., "Effect of a Nose Cavity on Heat Transfer and Flowfield over a Blunt Body at Mach 5," AIAA Paper 1994-2050, 1994.

[6] Yang, H. Q., and Antonison, M., "Unsteady Flow Field over a Forward-Looking Endoatmospheric Hit-to-Kill Interceptor," *Journal of Spacecraft and Rockets*, Vol. 35, No. 5, 1998, pp. 626–632. doi:10.2514/2.3395

[7] Hartmann, J., and Troll, B., "On a New Method for the Generation of Sound Waves," *Physics Review*, Vol. 20, No. 6, 1922, pp. 719–727. doi:10.1103/PhysRev.20.719

[8] Burbank, P. B., and Stallings, R. L., "Heat-Transfer and Pressure Measurements on a Flat Nose Cylinder at a Mach Number Range of 2.49 to 4.44," NASA TM X-221, 1959.

[9] Johnson, R. H., "Instability in Hypersonic Flow About Blunt Bodies," *The Physics of Fluids*, Vol. 2, No. 5, 1959, pp. 526–532. doi:10.1063/1.1705944

[10] Baysal, O., and Stallings, R. L., Jr., "Computational and Experimental Investigation of Cavity Flow Fields," *AIAA Journal*, Vol. 26, No. 1, Jan. 1988, p. 7. doi:10.2514/3.9842

[11] Marquart, E. J., and Grubb, J. P., "Bow Shock Dynamics of a Forward-Facing Nose Cavity," AIAA Paper 1987-2709, 1987.

[12] Huebner, L. D., and Utreja, L. R., "Experimental Flow Field Measurements of a Nose Cavity Configuration," Society of Automotive Engineers, Paper 871880, 1987.

[13] Yuceil, B., Dolling, D. S., and Wilson, D., "A Preliminary Investigation of the Helmholtz Resonator Concept for Heat Flux Reduction," AIAA Paper 1993-2742, 1993.

[14] Morgenstern, A., Jr., and Chokani, N., "Hypersonic Flow Past Open Cavities," AIAA Paper 1993-2969, 1993.

[15] Morgenstern, A., Jr., and Chokani, N., "Hypersonic Flow Past Open Cavities," *AIAA Journal*, Vol. 32, No. 12, 1994, pp. 2387–2393. doi:10.2514/3.12304

[16] Silton, S. I., and Goldstein, D. B., "Use of an Axial Nose-Tip Cavity for Delaying Ablation Onset in Hypersonic Flow," *Journal of Fluid Mechanics*, Vol. 528, No. 7, April 2005, pp. 297–321. doi:10.1017/S0022112004002460

[17] Silton, S. I., and Goldstein, D. B., "Ablation Onset in Unsteady Hypersonic Flow About Nose Tip with Cavity," *Journal of Thermophysics and Heat Transfer*, Vol. 14, No. 3, 2000, pp. 421–434. doi:10.2514/2.6540

[18] Engblom, W. A., Yuceil, B., Goldstein, D. B., and Dolling, D. S., "Hypersonic Forward-Facing Cavity Flow: An Experimental and Numerical Study," AIAA Paper 1995-0293, 1995.

[19] Engblom, W. A., Yuceil, B., Goldstein, D. B., and Dolling, D. S., "Experimental and Numerical Study of Hypersonic Forward-Facing Cavity Flow," *Journal of Spacecraft and Rockets*, Vol. 33, No. 3, 1996, pp. 353–359. doi:10.2514/3.26767

[20] Engblom, W. A., Ladoon, D., and Schneider, S., "Fluid Dynamics of Forward-Facing Cavity Flow," AIAA Paper 1996-0667, 1996.

[21] Engblom, W. A., and Goldstein, D. B., "Nose-Tip Surface Heat Reduction Mechanism," AIAA Paper 1996-0357, 1996.

[22] Engblom, W. A., and Goldstein, D. B., "Nose-Tip Surface Heat Reduction Mechanism," *Journal of Thermophysics and Heat Transfer*, Vol. 10, No. 4, 1996, pp. 598–606. doi:10.2514/3.835

[23] Satheesh, K., Jagadeesh, G., and Reddy, K. P. J., "High Speed Schlieren Facility for Visualization of Flow Fields in Hypersonic Shock Tunnels," *Current Science*, Vol. 92, No. 1, Jan. 2007, pp. 56–60.

[24] Olivier, H., "A Theoretical Model for the Shock Stand-off Distance in Frozen and Equilibrium Flows," *Journal of Fluid Mechanics*, Vol. 413, No. 1, June 2000, pp. 345–353. doi:10.1017/S0022112000008703

[25] Hollis, B. R., "User's Manual for the One-Dimensional Hypersonic Experimental Aero Thermodynamic (1DHEAT) Data Reduction Code," NASA CR-4961, 1995.

[26] Cook, W. J., and Felderman, E. J., "Reduction of Data from Thin Film Heat Transfer Gauge: A Concise Numerical Technique," *AIAA Journal*, Vol. 4, No. 3, 1966, pp. 561–562. doi:10.2514/3.3486

[27] Yuceil, B., and Dolling, D. S., "Effects of a Nose Cavity on Heat Transfer and Flowfield over a Blunt Body at Mach 5," AIAA Paper 1994-2050, 1994.

[28] Truitt, N. M., *Hypersonic Aerodynamics*, Ronald, New York, 1959.

[29] Mee, D. J., "Dynamic Calibration of Force Balances for Impulse Facilities," *Shock Waves*, Vol. 12, No. 6, 2003, pp. 443–456. doi:10.1007/s00193-003-0181-6

[30] Mee, D. J., "Uncertainties Analysis of Conditions in Test Section of the T4 Shock Tunnel," University of Queensland, Centre for Hypersonics, Research Report 4/93, Queensland, Australia, 1993.

M. Costello
Associate Editor